THE JOURNAL OF PHYSICAL CHEMISTRY C

pubs.acs.org/JPCC Article

Impact of Confinement on the Dynamics and H-Bonding Pattern in Low-Molecular Weight Poly(propylene glycols)

Agnieszka Talik,* Magdalena Tarnacka,* Monika Geppert-Rybczyńska, Barbara Hachuła,* Kamil Kaminski, and Marian Paluch

Cite This: J. Phys. Chem. C 2020, 124, 17607−17621

Read Online

ACCESS | Metrics & More | Article Recommendations | Supporting Information

ABSTRACT: Herein, we explored thermal properties, dynamics, wettability, and H-bonding pattern in various poly(propylene glycols) (PPG) of M_n = 400 g/mol confined into two types of nanoporous templates: silica (d = 4 nm) and alumina (d = 18 nm). Unexpectedly, it was found that the mobility of the interfacial layer and the depression of the glass transition temperature weakly depend on the pore size, surface functionalization, and wettability. However, interestingly, we have reported strengthening of the hydrogen bonds in samples confined in silica pores. Further, the unique annealing experiments on PPG-OH with the use of Fourier transform infrared spectroscopy revealed the reorganization of oligomers close to the interface and the formation of three distinct fractions, interfacial, intermediate, and bulk-like, in the infiltrated samples. These experiments might shed new light on the variation of the segmental/structural relaxation times due to annealing of materials of different molecular weights infiltrated into pores or deposited in the form of a thin layer.

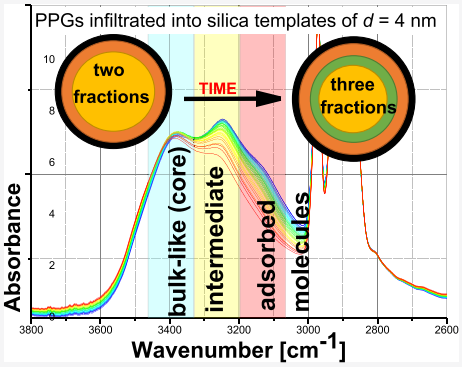

1. INTRODUCTION

The behavior of soft materials under nanoscale spatial restriction conditions became an attractive field of research over the past decades.[1,2] A special attention was focused on understanding in detail the molecular mechanisms governing the variation in the physicochemical properties of confined compounds.[3,4] Interestingly, as shown by numerous theoretical and experimental studies, these fluctuations arise mostly because of the competition of three major effects: surface interactions, finite size, and free volume.[5−8]

In fact, most investigations carried out to date demonstrated that the deviation in the molecular dynamics and phase/glass transition temperatures of confined materials is directly correlated with the size reduction realized by the decrease in both thicknesses of thin films and the pore diameter, d, of porous templates.[9] What is important, the positronium annihilation measurements carried out for liquids infiltrated into porous templates revealed that along with the change in the diameter of the nanocavities, a strong fluctuation in the free volume is noted.[10−12] At this point, it is worth quoting recent work by White and Lipson, who derived the cooperative free volume (CFV) model to describe general temperature and free volume-dependent structural relaxation behavior[10−12] of the bulk and confined materials. Briefly, one can stress that in this model, a group of molecules cooperate to obtain enough space for a rearrangement, and hence, the number of cooperating particles is inversely proportional to the free volume. This model was applied by Napolitano *et al.*[13] to explain enhanced dynamics of poly(4-chlorostyrene) and poly(2-vinylpiridine), prepared in a form of thin layers on the substrates differing in roughness. Moreover, recently, the CFV approach was used to describe segmental and chain dynamics of amino-terminated poly(propylene glycol) (PPG-NH_2) confined into native and silanized silica pores.[6] In this context, it is worthwhile to stress that a weak/negligible variation of the free volume below temperature connected to the vitrification of the interfacial molecules served as a base to formulate hypothesis that negative pressure controls dynamics of liquids confined in pores.[8,14−16]

Along with the development of the concepts relying on the variation in the finite size and free volume, an increasing number of papers highlighted the impact of the surface effects, as a dominant factor governing behavior of confined liquids. Especially, an increasing attention was paid lately to the processes occurring at the interface,[17−19] surface interactions,[20,21] and roughness.[13,22] One can recall that there were successful attempts to predict the direction and the magnitude of the confinement effect for various glass formers both deposited as thin films[20,23,24] and infiltrated within alumina [anodic aluminum oxide (AAO)] membranes[21,25] based on the

Received: May 6, 2020
Revised: July 7, 2020
Published: July 9, 2020

interfacial energy, γ_{SL}. As shown, the higher γ_{SL}, the greater deviation from the bulk behavior is expected.[21,25]

Nevertheless, it should be noted that although finite size and surface effects on the dynamics of nanospatially confined liquids are very often considered separately, recent works indicated some kind of entanglement between them. In this context, it is worthwhile to remind recent atomic force microscopy measurements performed for glycerol incorporated within alumina membranes of d = 10 nm,[26] demonstrating that surface tension and most likely interfacial tension γ_{SL} varies with the surface curvature of applied nanochannels.[27−29] Moreover, a close correlation between both effects is also well illustrated in the case of the dielectric studies on PPG infiltrated within controlled porous glasses of various pore diameters (d = 2.5−20 nm).[30−32] As shown, the glass transition temperature, T_g, of infiltrated PPG revealed a nonlinear (parabolic) dependence, where the rise of T_g noted for smaller pore diameter (d < 3 nm) was discussed in terms of the adsorption effects overcoming the confinement one. On the other hand, in the case of various PPG derivatives within silica pores characterized by a little larger pore sizes (d = 4−8 nm),[3,5,6] a linear reduction of T_g with increasing degree of confinement was observed for both native and silanized templates. This might indicate that the impact of the surface effects should be often discussed together with the finite size (especially the pore curvatures) which might induce changes in the surface interactions and also should be taken into account to predict the behavior of the confined liquids.[33−36]

In this article, we probe the counterbalance between the confinement and surface effects on the chemically modified poly(propylene glycols) (PPG) derivatives of molecular weight M_n = 400 g/mol incorporated into silica (native and silanized) and alumina (AAO) membranes of various pore diameters (d = 4 nm and d = 18 nm) measured using dielectric and infrared (IR) spectroscopy as well as differential scanning calorimetry (DSC). These investigations allowed to get insight into the variation in wettability, dynamics, and H-bonded pattern in the spatially restricted samples infiltrated into both kind of membranes.

2. MATERIALS AND METHODS

2.1. Materials. Poly(propylene glycol) (PPG-OH) and poly(propylene glycol) bis(2-aminopropyl ether) (PPG-NH_2) of M_n = 400 g/mol with purity higher than 98% were supplied by Sigma-Aldrich. The nanoporous alumina oxide membranes used in this study (supplied from InRedox) are composed of uniaxial channels (open from both sides) with well-defined pore diameter, $d \sim 18 \pm 2$ nm, thickness $\sim 50 \pm 2$ μm, and porosity $\sim 12 \pm 2$%. Details concerning pore density, distribution, and so forth can be found on the Webpage of the producer.[37] The preparation of native and functionalized silica templates are presented in the Supporting Information file. Finally, it should be mentioned that density of the confined materials is assumed to be approximately the same as the bulk material at room temperature (RT).

2.2. Methods. *2.2.1. Broadband Dielectric Spectroscopy (BDS).* Isobaric measurements of the complex dielectric permittivity $\varepsilon^*(\omega) = \varepsilon'(\omega) - i\varepsilon''(\omega)$ were carried out using the Novocontrol Alpha dielectric spectrometer over the frequency range from 10^{-1} Hz to 10^6 Hz at ambient pressure. The temperature uncertainty controlled by Quatro Cryosystem using the nitrogen gas cryostat was better than 0.1 K. Dielectric measurements of native silica and silanized membranes (of d = 4 nm) filled with PPG-OH, PPG-NH_2, and PPG-OCH_3 were placed between stainless steel plates having 5 mm diameter. Moreover, dielectric measurements on empty membranes were also carried out to evaluate their contribution which turned out to be negligible, to the measured loss spectra (see Figure S1 in the Supporting Information file).

2.2.2. Differential Scanning Calorimetry. Calorimetric measurements were carried out using a Mettler-Toledo DSC apparatus (Mettler-Toledo International, Inc., Greifensee, Switzerland) equipped with a liquid nitrogen cooling accessory and an HSS8 ceramic sensor. Temperature and enthalpy calibrations were investigated using indium and zinc standards, and the heat capacity, C_p, calibration was performed using a sapphire disc. After placing crushed templates in the aluminum crucibles, they were sealed and measured over a wide temperature range with cooling and heating rates equal to 10 K/min. Each experiment was repeated three times. In addition, measurements on empty membranes were carried out (please see Figure S1 in the Supporting Information file). It was found that in the range of the studied temperature, there is no change in heat flow, indicating no contribution from the silica and alumina to the heat capacity jumps detected for the membranes filled with studied PPGs.

2.2.3. Fourier Transform Infrared Spectroscopy (FTIR). The Nicolet iS50 FTIR spectrometer (Thermo Scientific) was used to measure the FTIR spectra of the bulk and the confined PPGs samples. FTIR spectra were recorded in the 4000−1300 cm^{-1} frequency region with a spectral resolution of 4 cm^{-1}. The limited spectral range resulted from the detector saturation in the region of Si−O and Al−O stretching vibrations. Each spectrum was obtained by averaging 32 scans. The measurements were carried at RT (293 K) and glass transition temperature (T_g) determined from the BDS measurements. The low-temperature IR spectra were obtained by using a liquid nitrogen-cooled Linkam THMS 600 stage (the temperature accuracy of ±0.1 °C), which was adapted to the Nicolet spectrometer. The measurements were performed at a cooling rate of 10 °C/min in a nitrogen atmosphere. The time-dependent IR spectra were measured at equal intervals, that is, every 1 min after the temperature stabilization at T = 183 K. The FTIR spectra of native, silanized silica, and alumina membranes were measured and are presented in Figure S1. The −OH stretching band decomposition was performed using the MagicPlot 2.9.3 software (MagicPlot Systems, LCC). The band occurring between 3050 and 3950 cm^{-1} was decomposed with the use of several Gaussian functions adjusting the intensity and the width of the fitting curves. The two wavelength intervals at *ca.* 2400−2500 and 3050−3950 cm^{-1} (excluding the spectral region of the CH stretching band) were used for fitting. All spectral parameters were left free during the fitting procedure. The "best fit" was considered when the statistical parameter R was the lowest. One can stress that although the amount of −OH groups on silica surface can vary with the surface preparation method,[38] the peak position connected to the vibration of this moiety is located at ν_{Si-OH} ~3748 cm^{-1}. Interestingly, at this region, we did not observe any contribution from the PPG infiltrated into pores. Thus, there is no need to consider the influence of Si−OH groups from the silica membrane during the deconvolution process. In the case of alumina templates, the maximum of the OH band is found at 3640 cm^{-1} in the range of weak H-bonded bulk-like PPG-OH molecules. However, the analysis of the OH vibration in this frequency regime does not affect a discussion

https://dx.doi.org/10.1021/acs.jpcc.0c04062
J. Phys. Chem. C 2020, 124, 17607−17621

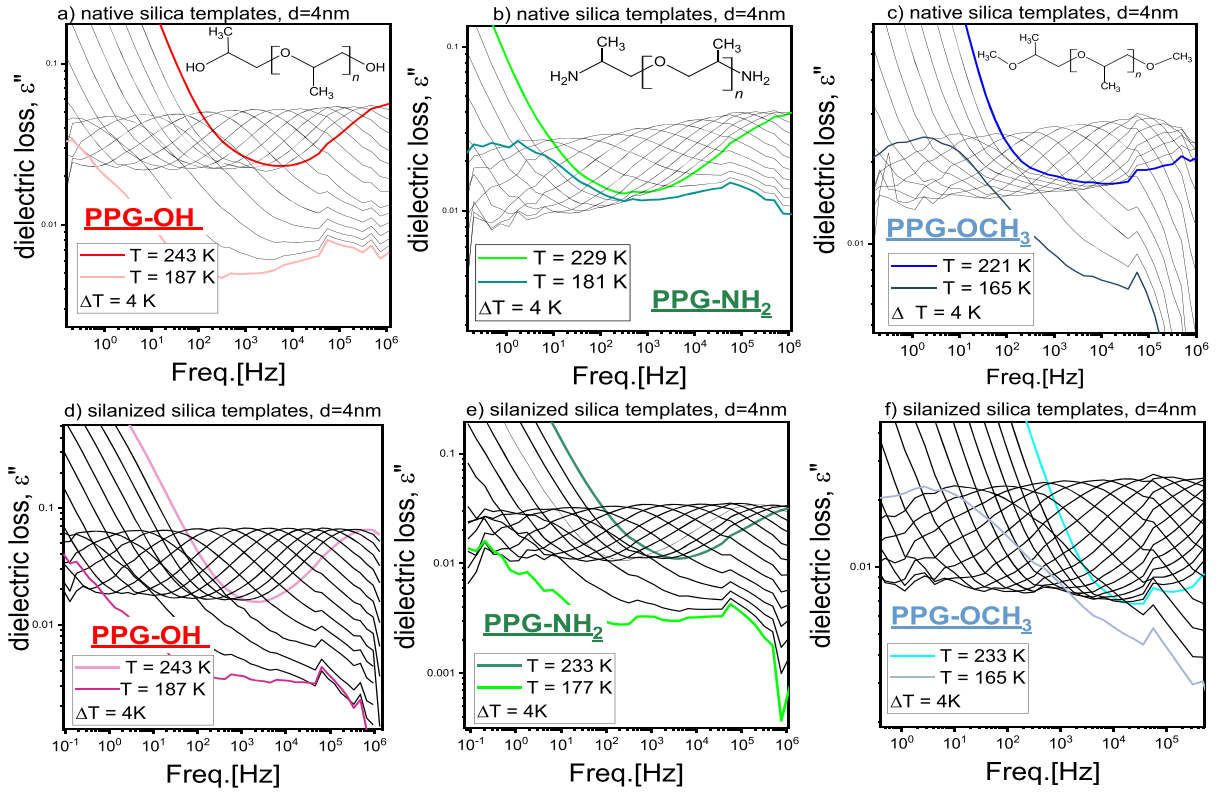

Figure 1. Dielectric loss spectra for various PPG derivatives confined into native (a–c) and silanized (d–f) silica templates of d = 4 nm, measured above T_g. Black and color curves correspond to the different temperatures. The chemical structures of investigated substances are presented as insets (a–c).

about existence of three different layers of PPG-OH infiltrated in silica and alumina native pores. The CH band components were also excluded from the decomposition of the OH band as the fitting of a poorly resolved broad OH band with multiple component is always subject to a large error. Thus, fitting even more bands (*i.e.,* the CH signals) can only worsen the final deconvolution result.

2.2.4. Surface Tension and Contact Angle Measurements. The surface tension of liquids γ_L (pendant drop method) and contact angle θ were measured with the DSA 100S Krüss Tensiometer, GmbH Germany. The description of the instrument and procedures has been presented previously.[39,40] The measuring procedure at T = 298.2 K for all substances has been repeated dozen or more times. The temperature measurement uncertainty was ±0.1 K. The precision of contact angle measurements was 0.01°, and the estimated uncertainty was ±1.5°, whereas the uncertainty of surface tension was ±0.1 mN·m^{-1}. Density, ρ, required for the surface tension experiment was measured with an Anton Paar DMA 5000M densimeter with the uncertainty not worse than 0.0001 g·cm^{-3}. For the surface energy estimation of native and silanized silica, some of the following liquids were considered: water, ethylene glycol, diiodomethane, and glycerol. The dispersive and nondispersive part in the surface tension for these substances were taken from ref 21. The calculated surface energy for native silica was 67.6 mJ/m^2 with the dominant nondispersive part equaling 66.6 mJ/m^2. For the silanized surface, the respective value was 25.3 mJ/m^2 with the as-expected dominant and the dispersive component was 22.8 mJ/m^2.

3. RESULTS AND DISCUSSION

Dielectric loss spectra of studied poly(propylene) glycols (PPG) terminated by three different groups, −OH, −NH_2, and −OCH_3, incorporated into native and silanized silica templates (of d = 4 nm) are shown in Figure 1. Note that dielectric spectra for bulk substances, taken from ref 41, are presented in the Supporting Information file. In all cases, dielectric data revealed the presence of the dc conductivity related to the charge transport and the segmental (α) relaxation at higher frequencies reflecting the cooperative motions of the molecules and responsible for the liquid-to-glass transition. Herein, one can stress that because of low molecular weight, M_n < 1000 g/mol, of studied PPG,[16,25] the additional mobility related to the fluctuations of the end-to-end vector of the chain ends called usually as the normal mode process cannot be observed (see Figure 1).

One can also mention that often for the materials confined within silica membranes, the appearance of the interfacial process, reflecting reorientational motions of the polymers adsorbed at the surface of the pore walls, are widely reported. Interestingly, this specific relaxation is not observed in the case of studied PPG, independently to the applied porous matrix and functionalization (see Figure 1). This finding agrees with the data published by Arndt *et al.*,[1] who studied salol and glycerol, differing in the number of hydroxyl units, infiltrated in silica pores of d = 4–8 nm. They found that while a reorientation of the adsorbed molecules can be detected for the former system (salol with one −OH group), it is not visible for the latter alcohol (glycerol with three −OH moieties). It was proposed to link this experimental observation to the balance between timescales of the exchange process between

https://dx.doi.org/10.1021/acs.jpcc.0c04062
J. Phys. Chem. C 2020, 124, 17607−17621

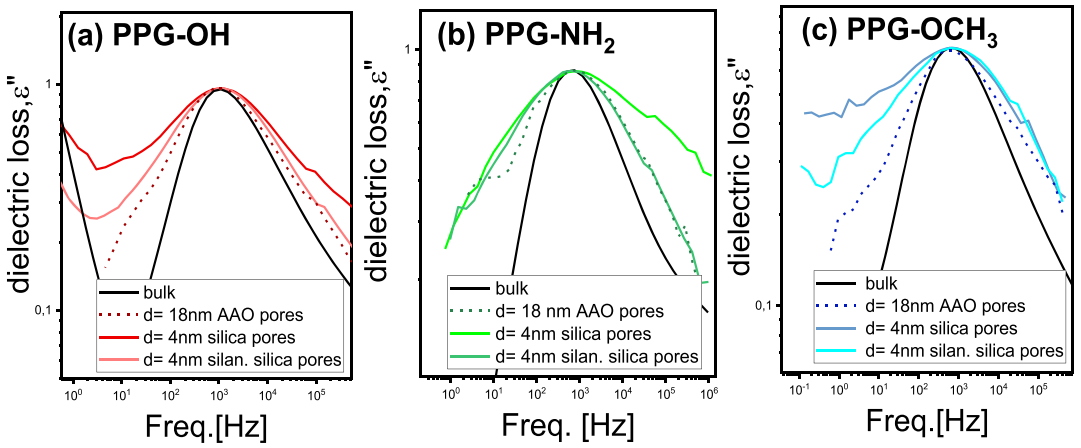

Figure 2. Segmental α-loss peaks collected at comparable τ_α for bulk and confined PPG-OH (a), PPG-NH_2 (b), and PPG-OCH_3 (c). Data for PPG derivatives confined within AAO membranes of d = 18 nm were taken from ref 41.

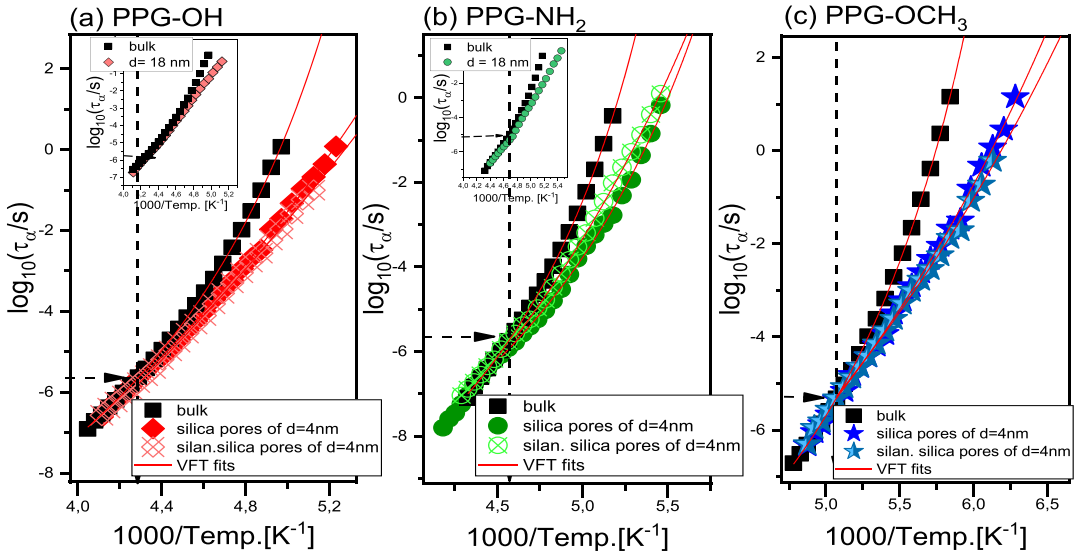

Figure 3. Structural relaxation times plotted *vs* inverse temperature for all studied PPG derivatives infiltrated into silica and alumina templates. Red solid lines are the best fits to the VFT equations (eq 2). Data for PPG derivatives confined within AAO membranes of d = 18 nm were taken from ref 41.

core and interfacial molecules and experiments.[1] Note that if the exchange between both fractions is either fast or slow with respect to the time of the experiments, the interfacial process can be detected or not in the loss spectra respectively. However, we suppose that this phenomenon might be also somehow related to the number of hydroxyl units within the sample. Once the number of this particular moieties is equal to unity, the interfacial process is well visible as a separate loss peak, while in the case of materials with two or more −OH groups (*i.e.*, glycerol or PPG-OH), this mode vanishes. This pattern of behavior is similar to what was previously found in the case of bulk alcohols, where for monohydroxy alcohols, an additional Debye relaxation (related to the formation of the hydrogen bonding supramolecular structure) is observed; while in polyacohols, there is no trace of this kind of mobility in the collected dielectric spectra.[26] Nevertheless to explain if there is any relationship between the appearance of the Debye process in monohydroxyalcohols and interfacial process in liquids confined in pores, further studies are required.

In Figure 2, α-loss peaks of the bulk and confined samples were superimposed at the constant segmental relaxation times, τ_α, for all investigated compounds. As shown, the shape of the α-loss peaks significantly broadens with increasing confinement because of the increased dynamical heterogeneity induced by the additional interactions with the pore walls.[15,42] However, it should be pointed out that the α-loss peak of PPGs within the functionalized (silanized) silica templates is, interestingly, narrower than the one recorded for PPG infiltrated into native silica. In general, this might suggest a change in the surface interactions between hydrophobic (silanized) and hydrophilic (native) templates. Note that the broader α-loss peaks within native templates might also be a result of the dynamical perturbation introduced by stronger interactions between the substrate and adsorbed molecules. It is worth mentioning that similar observations were made for other low and high molecular weight samples infiltrated in pores.[1,25,31,42]

To explore in more detail, the molecular dynamics of confined materials and collected dielectric spectra were analyzed using Havriliak−Negami (HN) function with the conductivity term[43]

https://dx.doi.org/10.1021/acs.jpcc.0c04062
J. Phys. Chem. C 2020, 124, 17607−17621

Table 1. Values of the GlassTransition Temperatures, Changes in Heat Capacity, and Thickness of the Interfacial Layer Calculated for Bulk and Confined Systems Collected from Calorimetric and Dielectric Measurements[a]

	$T_{g,core}$ [K]	$T_{g,interfacial}$ [K]	$\Delta T_{g,core}$ [K]	$\Delta T_{g,interfacial}$ [K]	$T_{g,core}$ [K]	$T_{g,int}$ [K]	$\Delta C_{p,core}$ [J/g K]	$\Delta C_{p,int}$ [J/g K]	ξ [nm]
				PPG-OH					
bulk	196				199				
native SiO_2	183	231	−13	35	185	226	0.393	0.651	0.9
silanized SiO_2	179	230	−17	34	190	221	0.284	0.335	0.52
				PPG-NH_2					
bulk	187				193				
native SiO_2	176	221	−11	34	178	222	0.413	0.945	0.89
silanized SiO_2	176	217	−11	30	184	217	0.327	0.278	0.37
				PPG-OCH_3					
bulk	169				173				
native SiO_2	156	197	−13	28	159	187	0.171	0.353	0.86
silanized SiO_2	154	197	−15	28	163	190	0.215	0.423	0.97

[a]Data for bulk PPG derivatives taken from ref 41.

$$\varepsilon(\varpi)'' = \frac{\sigma_{dc}}{\varepsilon_0 \varpi} + \frac{\Delta\varepsilon}{[1 + (i\varpi\tau_{HN})^{\alpha_{HN}}]^{\beta_{HN}}} \quad (1)$$

where α_{HN} and β_{HN} are the shape parameters representing the symmetric and asymmetric broadening of given relaxation peaks, $\Delta\varepsilon$ is the dielectric relaxation strength, τ_{HN} is the HN relaxation time, ε_0 is the vacuum permittivity, and ϖ is an angular frequency ($\varpi = 2\pi f$). Note that τ_α was estimated from τ_{HN} accordingly to the equation given in ref 44. Determined segmental relaxation times were plotted as a function of inverse temperature and shown in Figure 3. As illustrated, the $\tau_\alpha(T)$-dependences of all confined PPG is a bulk-like at a high-temperature region. However, below the temperatures denoted as $T_{g,interfacial}$, they start to deviate from the bulk behavior irrespectively of the sample and porous template. As widely reported, this phenomenon is related to the vitrification of the materials adsorbed to the pore walls.[1,6,15,45] In this context, one can mention about "two-layer" or "core−shell" models often used to discuss/interpret results of molecular dynamics simulations or quasi-elastic neutron scattering investigations.[46] In view of these simplified approaches, liquids infiltrated in pores are considered as consisted of the molecules located in the center of the pores ("core") and adsorbed to the walls ("interfacial"). They are characterized by different densities and mobilities because of additional interactions with the solid substrate.[1,60]

Analysis of the data presented in Figure 3 unexpectedly revealed that the bifurcation of $\tau_\alpha(T)$-dependences of the confined PPGs occurs at similar τ_α (log $\tau_\alpha \sim -5.5$) independently to the terminal groups, applied porous template, and functionalization (silanized or native). It is worth adding that the deviation of $\tau_\alpha(T)$-dependences of PPGs infiltrated into alumina templates also occurs at comparable τ_α, the same as in the case of material confined in silica pores (see insets of Figure 3a,b). Note that data for PPG derivatives within AAO membranes of d = 18 nm were taken from ref 41. In this context, it should be mentioned that the similar finding has been recently reported for a primary and secondary monohydroxy alcohols incorporated within alumina and silica pores. It was shown that the temperature dependences of the Debye relaxation times, τ_D (reflecting the mobility of supramolecular self-assemblies[47,48]), deviate from the bulk-like behavior at approximately the same τ_D irrespectively of the porous template, chemical structure, and architecture of the supramolecular structures formed in the studied systems.[49] Moreover, recently Tu *et al.*[50] found the same scenario in ionic liquids confined in the native and functionalized alumina pores. This indicates that the change in the porous template, hydrophobicity, or hydrophilicity of the pore surface does not affect segmental dynamics of the interfacial layer to much because the bifurcation of $\tau_\alpha(T)$-dependences of the core PPGs occurs at similar τ_α (log $\tau_\alpha \sim -5.5$). Interestingly, this agrees with the molecular dynamics simulations showing that although functionalization of the pore walls influences on the dynamics of the interfacial molecules, this effect is not significant.[51]

To estimate the glass transition temperature, T_g, obtained, data presented in Figure 3 were fitted using the Vogel−Fulcher−Tamman (VFT) equation[52−54]

$$\tau_\alpha = \tau_\infty \exp\left(\frac{D_T T_0}{T - T_0}\right) \quad (2)$$

where τ_∞ is the relaxation time at finite temperature, D_T is the fragility parameter, and T_0 is the temperature, where τ goes to infinity. It should be mentioned that the two VFT functions were applied for the confined systems because of the observed deviation in the slope of $\tau_\alpha(T)$-dependencies. The first one (high temperature VFT) was used only for an accurate determination of a point (temperature), at which the slope changes (related to the vitrification of the interfacial layer and denoted as $T_{g,interfacial}$), while, the glass transition temperatures of the confined samples (in this case of the core polymers, $T_{g,core}$) were estimated from the second, low-temperature VFT fits. The values of all calculated glass transition temperatures are listed in Table 1. Note that $T_{g,core}$ is defined as a temperature at which τ_α = 100 s. As observed, irrespective of the terminal group and applied template, estimated values of $T_{g,interfacial}$ are comparable. Moreover, the same scenario can also be observed in the case of $T_{g,core}$ (within the experimental uncertainty). This implies that the performed surface modification (silanization) along with the variation in the porous matrix and pore diameter have for some reason a marginal impact on the segmental dynamics of infiltrated PPG derivatives. This observation seems to be quite surprising taking into account that to date, a simple silanization of silica, leading to a prominent change of the polarity, specific interactions (H-bonds), hydrophilicity, and hydrophobicity, generally induced difference in the behavior of materials incorporated within native and functionalized templates.[30−32]

https://dx.doi.org/10.1021/acs.jpcc.0c04062
J. Phys. Chem. C 2020, 124, 17607−17621

To better understand reported findings, we further measured contact angles, θ, and surface tensions, γ_L, and calculated the interfacial tension, γ_{SL}, prior and after surface modification.[55,56] The estimated values of contact angles and surface tensions for all studied materials and surfaces are listed in Table 2. As

Table 2. Contact Angles (θ), Surface Tension (γ_L), and Interfacial energy (γ_{SL}) Estimated at RT T = 298 K for All Investigated Systems[a]

sample	θ [deg]	γ_L [mN·m^{-1}]	γ_{SL} [mN·m^{-1}]
	Alumina Surface		
PPG-OH	6.2	32.4	26.7
PPG-NH_2	5.4	31.6	27.6
PPG-OCH_3	6.0	22.8	36.3
	Silica Native Surface		
PPG-OH	26.3	32.4	38.5
PPG-NH_2	24.7	31.6	38.9
PPG-OCH_3	5.8	22.8	45
	Silica-Silanized Surface		
PPG-OH	37.9	32.4	−0.2
PPG-NH_2	28.7	31.6	−2.3
PPG-OCH_3	7.4	22.8	2.8

[a]Data for the alumina surface were taken from ref 41.

observed, the contact angles of investigated samples change significantly depending on their chemical structure and type of matrices. Both PPG-OH and PPG-NH_2 are characterized by comparable contact angles on native silica surface ($\theta \sim 25°$), which indicates good wettability. However, their θ increases because of surface modification even up to $\theta \sim 37°$ for PPG-OH on the silanized silica surface. The increase of θ suggests, in fact, the reduction of wettability on the modified interface with respect to the native one, more likely because of the strong change in the interactions between host and guest materials. In this context, one can also add that in the case of the alumina surface, the contact angle of both PPG-OH and PPG-NH_2 is extremely low ($\theta \sim 6°$ indicates they wet this surface perfectly). On the other hand, PPG-OCH_3 surprisingly seems to wet all surface in a similar manner as its contact angle remains comparable for all surfaces ($\theta \sim 6–7°$).

Next, we estimated interfacial energy, γ_{SL}, according to the Young equation ($\gamma_{SL} = \gamma_S - \gamma_L \cos\theta$, where γ_S is the surface energy).[55] Calculated values of γ_{SL} are listed in Table 2. Interestingly, for the silanized matrices, we noted low values of interfacial energies for all examined compounds. This indicates a clear change in the interfacial interactions between materials and functionalized silica in the vicinity of the pore walls, where the dispersive interactions prevail.[56,57] In this context, one can recall studies on the thin films that revealed that the higher value of γ_{SL}, the greater deviation from the bulk behavior because of the reduced mobility at the interface.[20,23,24] This approach was further applied to the porous materials by Alexandris *et al.*[21] for several polymers infiltrated within AAO membranes.[21,58] As shown, the increase of the difference between the glass transition temperature, T_g, of the bulk and confined samples, ΔT_g, enlarges with the rise of the interfacial tension. This relationship was well quantified by the systematic measurements of the wettability, allowing us to calculate the interfacial energy, γ_{SL}, and T_g of the spatially restricted polymers.[21,25] Further studies indicated that higher γ_{SL} implies reduced mobility of the interfacial layers that consequently leads to greater depression of $T_{g,core}$ in pores.[25]

In Figure 4, we have plotted the estimated values of γ_{SL} *versus* $\Delta T_{g,core}$ and $\Delta T_{g,interfacial}$ calculated for PPGs infiltrated

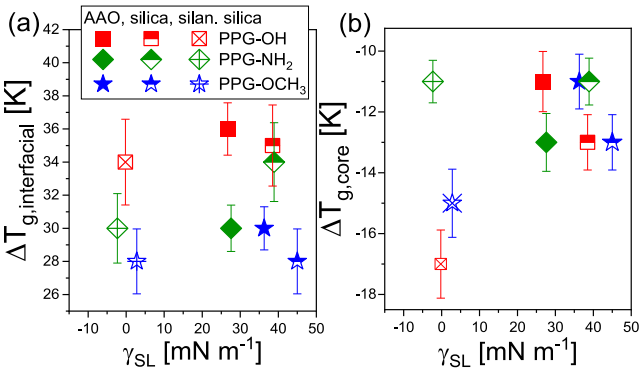

Figure 4. $\Delta T_{g,interfacial}$ (a) and $\Delta T_{g,core}$ (b) calculated from dielectric data, plotted as a function of the interfacial energy for studied PPG derivatives incorporated into AAO (of d = 18 nm) and native and silanized silica (of d = 4 nm) pores. Data for PPGs confined within AAO membranes of d = 18 nm were taken from ref 41.

into alumina (d = 18 nm) and silica (d = 4 nm) templates. Note that $\Delta T_{g,core}$ is the difference between $T_{g,core}$ and T_g of bulk ($\Delta T_{g,core} = T_{g,core} - T_g$), while $\Delta T_{g,interfacial}$ is the discrepancy between $T_{g,interfacial}$ and T_g of bulk ($\Delta T_{g,interfacial} = T_{g,interfacial} - T_g$). As shown in Figure 4, both $\Delta T_{g,core}$ and $\Delta T_{g,interfacial}$ of all investigated PPG incorporated in porous matrices are similar (within experimental uncertainty). Surprisingly, despite a clear variation in wettability, interfacial energy and pore size (d = 18 nm *vs* d = 4 nm), no differences between studied systems infiltrated within alumina and silica templates can be observed. In this context, one can remind that recent studies on various PPG derivatives infiltrated into AAO membranes revealed that γ_{SL} weakly depends on both their terminal groups and molecular weight, M_n, whereas $\Delta T_{g,interfacial}$ changes with both these factors.[59] The finding discussed above clearly indicates that although the interfacial tension is a very useful parameter to predict depression of the glass transition temperature of the polymers infiltrated into porous media, it is not sufficient to understand the complex dynamics of such heterogeneous systems. Therefore, the contribution of other factors, possibly related to the variation in the density packing and roughness of the pore walls must be considered as well.

In the next step, we have performed additional DSC measurements to support/confirm results of dielectric investigations. Thermograms recorded for all studied PPG derivatives incorporated within silica templates are presented in Figure 5. As illustrated, all samples exhibit the presence of the two endothermic processes, related to the vitrification of the interfacial (denoted as $T_{g,interfacial}$) and "core" (labeled as $T_{g,core}$) molecules located above and below T_g of the bulk material, respectively (so-called the double glass-transition phenomenon).[42,60,61] It should be pointed out that even for PPGs infiltrated into silanized silica templates characterized by the extremely low value of the interfacial energy, ($\gamma_{SL} \sim 2$ mN·m^{-1}), double glass transition was detected. The value of $T_{g,interfacial}$ and $T_{g,core}$ obtained from DSC measurements for confined materials and also T_g of the bulk samples were added to Table 1. Although, there are some discrepancies between the value of T_g determined from calorimetric and dielectric measurements, which can be due to the difference in the

https://dx.doi.org/10.1021/acs.jpcc.0c04062
J. Phys. Chem. C 2020, 124, 17607−17621

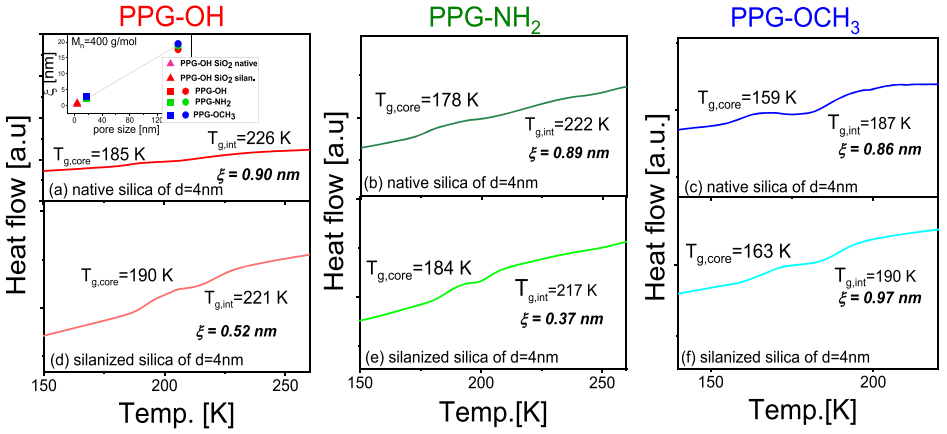

Figure 5. DSC thermograms together with the estimated length scale of the interfacial layer, ξ (eq 3), obtained for PPGs incorporated into both native and silanized silica templates; as the inset, the length scale of interfacial layer (ξ) plotted *vs* pore diameter for PPG-OH, PPG-NH_2, PPG-OCH_3 confined into AAO (d = 150, 18 nm) and SiO_2 (d = 4 nm, native and silanized) membranes.

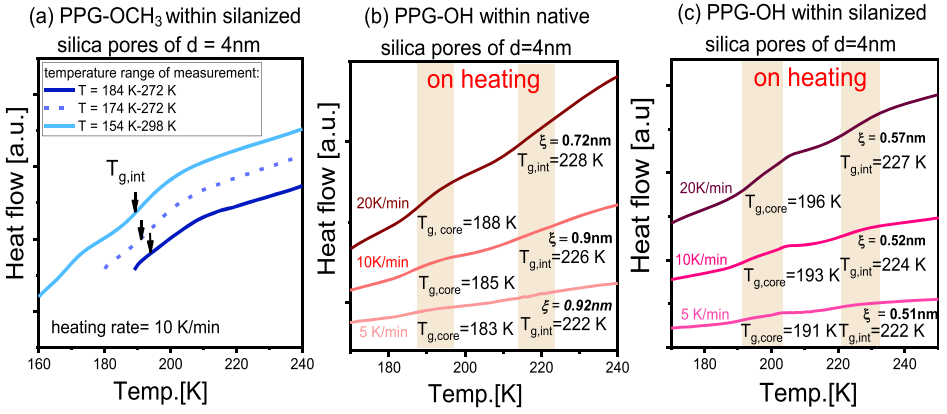

Figure 6. DSC thermograms obtained for confined systems: (a) thermal history of PPG-OCH_3 confined into d = 4 nm of silanized silica pores and examined for selected temperatures above $T_{g,core,}$ at constant heating rate = 10 K/min; (b,c) heating traces obtained for PPG-OH confined into native and silanized silica pores following different cooling rates (5−20 K/min).

heating/cooling rate applied in both methods[41] they are similar.

Furthermore, we also determined the length scale of the interfacial layer, ξ, which also can be obtained directly from DSC measurements[60]

$$\xi = \frac{d}{2}\left[1 - \left(\frac{\Delta C_{p,\text{interfacial}}}{\Delta C_{p,\text{interfacial}} + \Delta C_{p,\text{core}}}\right)^{1/2}\right] \quad (3)$$

where d is the pore diameter; $\Delta C_{p,\text{core}}$ and $\Delta C_{p,\text{interfacial}}$ are the changes of the heat capacity at $T_{g,\text{core}}$ and $T_{g,\text{interfacial}}$. Note that the application of eq 3 requires the following assumptions: (i) the volume of the material in the surface layer is proportional to the step change of its heat capacity, (ii) the density of the incorporated material does not change along the pore radius, and (iii) the shape of the pore is cylindrical. The values of the heat capacity and calculated thickness of the interfacial layer are listed in Table 1 and Figure 5. As observed, the estimated ξ reaches similar values for all PPGs when infiltrated into native silica membranes (within experimental uncertainty), which are comparable to those ones reported earlier for 2E1H[8] or for monohydroxy alcohols,[49] where the value of ξ oscillated around ∼1 nm. However, after the silanization, ξ decreases for PPG-OH and PPG-NH_2 because of change in the interfacial interaction (*i.e.*, suppression of H-bonds). In contrast, in the case of PPG-OCH_3, the length scale of the interfacial layer increases after the surface modification, most likely due to increased surface-dispersive interactions.[56,57] One can add that according to the literature, ξ varies dependently to the type and strength of interactions, including hydrogen bonds.[1] It is also worthwhile to add that ξ of low-molecular-weight PPG incorporated within the alumina templates of d = 18−150 nm increases with the pore size but was relatively independent to the terminal end-groups of studied oligomers. In addition, we compared and plotted the thickness of the interfacial layer estimated for the PPG oligomer infiltrated into pores, made of silica and alumina having different pore sizes; please see the inset in Figure 5. Data for PPG infiltrated in AAO were taken from ref 41. This graph clearly illustrates that there is a linear relationship between thickness of the interfacial layer and pore diameter, d, which indicates some entanglement between both parameters. Moreover, it is worthwhile to stress that the interfacial layer estimated from calorimetry for the samples infiltrated into larger pores barely agree with those calculated for the thin films. In this particular case, ξ is around ∼2−3 nm and weakly depends on the film thickness.[62] Hence, one can state that the interfacial layer determined from calorimetry for the infiltrated systems is related to the length scale obeying molecules/polymers of much slower dynamics with respect to

https://dx.doi.org/10.1021/acs.jpcc.0c04062
J. Phys. Chem. C 2020, 124, 17607−17621

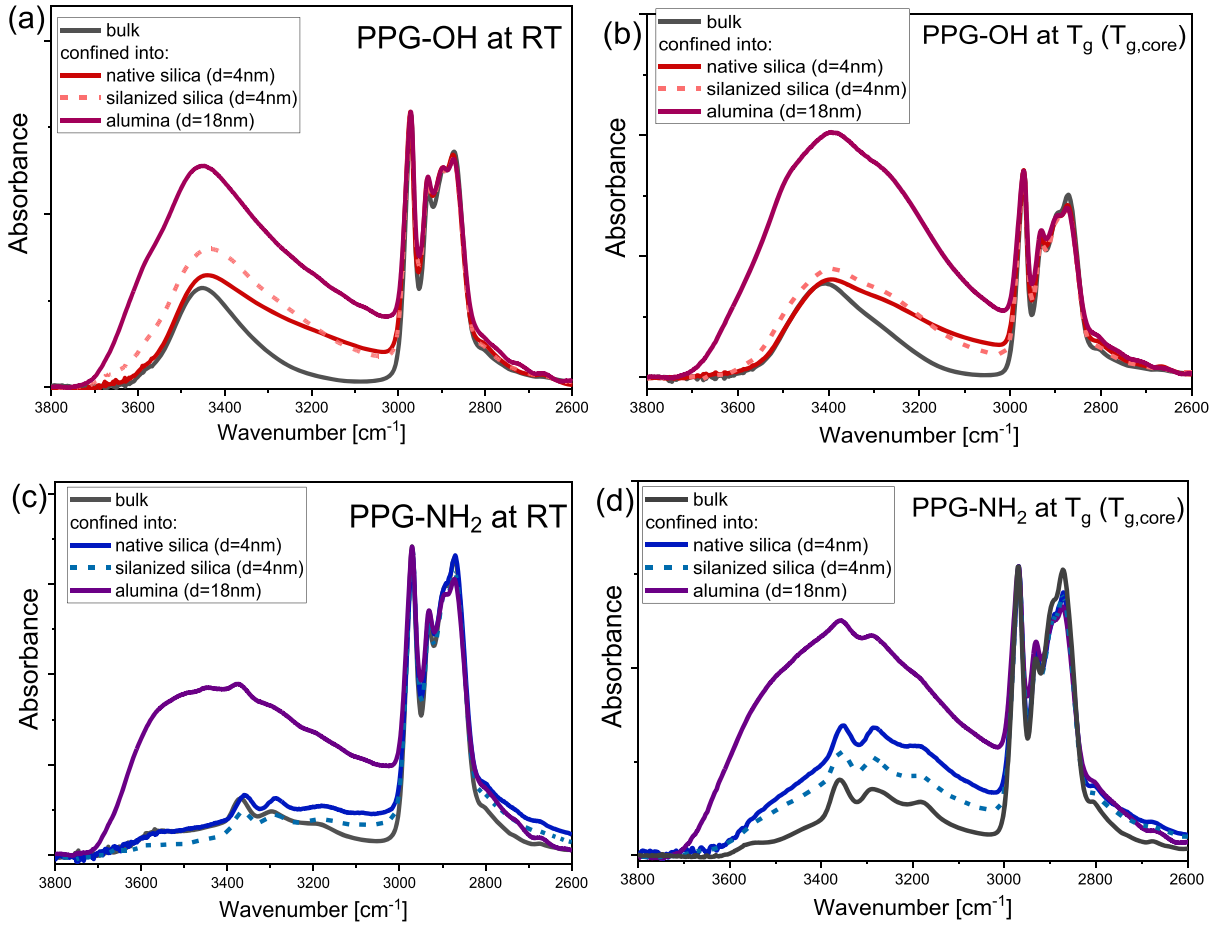

Figure 7. FTIR spectra of bulk (black) and confined PPG-OH (a,b) and PPG-NH_2 (c,d) measured in the ν_{X-H} and the ν_{C-H} vibration regions at RT (a,c) and at glass transition temperature (b,d). The spectra were normalized to the C−H absorption peak at around 2970 cm^{-1}.

the core material because of the perturbation introduced by interactions with the substrate.

Taking advantage of the fact that both glass transition temperatures were well visible in the thermograms collected for the PPG confined in silica and alumina pores, we decided to find out whether this material will behave in a similar way as entangled *cis*-1,4-polyisoprene (PI) infiltrated in AAO membranes.[58] Just to mention that in this particular case, Politidis *et al.* have demonstrated that $T_{g,interfacial}$ is conditional and can be detected only for the samples cooled down below $T_{g,core}$; this observation allowed them to hypothesize that $T_{g,core}$ is a spinodal temperature. Therefore, as a subsequent point of our studies, we have performed additional calorimetric measurements using several temperature protocols to investigate the behavior of low-molecular-weight PPG derivatives infiltrated into silica templates of d = 4 nm to check how does various thermal histories influence the existence of the double glass-transition phenomenon. For this purpose, we carried out three cooling scans followed by heating in accordance to the following protocols: (1) cooling down to 184 K (deep below $T_{g,core}$), (2) cooling to 174 K (between both detected T_gs), and (3) again cooling down to 184 K. Representative DSC thermograms obtained for infiltrated PPG-OCH_3 are shown in Figure 6a. Interestingly, in contrast to the data reported in ref 58, a prominent $T_{g,interfacial}$ appears in all registered thermograms questioning assignments of the low glass transition temperature as the spinodal temperature. To explain the discrepancy between results reported herein and the ones presented in ref 58, one should consider (i) different molecular weights of studied polymers (we focused only on PPG of M_n = 400 g/mol), (ii) various porous templates (characterized by different finite size and surface interactions), and (iii) significantly different wettabilities and interfacial tension of PI and PPG on the alumina and silica surfaces.

Furthermore, we also carried out a series of DSC measurements with different heating rates, 5−20 K/min. Selected thermograms recorded for PPG-OH incorporated within native and silanized templates of d = 4 nm are presented in Figure 6b,c. As expected, both T_gs shift toward higher temperatures with the increasing heating rate. Additionally, we also observed that the length scale of the interfacial layer, ξ, increases with lowering the heating rate in the case of PPG-OH infiltrated into native silica templates (Figure 6b); whereas for PPG-OH within the silanized silica templates, ξ seems to remain constant independently to the applied heating rate (Figure 6c). This simple experiments indicated that although the dynamics of the interfacial layer is not so much different in the vicinity of the functionalized pore walls, the length scale of the molecules adsorbed to the pore walls is affected in a more significant way.

As a final point of our investigations, we have carried out additional FTIR measurements to gain information about the H-bonded pattern in the samples confined within silica and alumina nanopores. Figure 7 shows the comparison of FTIR spectra of bulk PPG-OH, PPG-NH_2, and samples infiltrated in alumina and silica (native and functionalized) templates at RT

https://dx.doi.org/10.1021/acs.jpcc.0c04062
J. Phys. Chem. C 2020, 124, 17607−17621

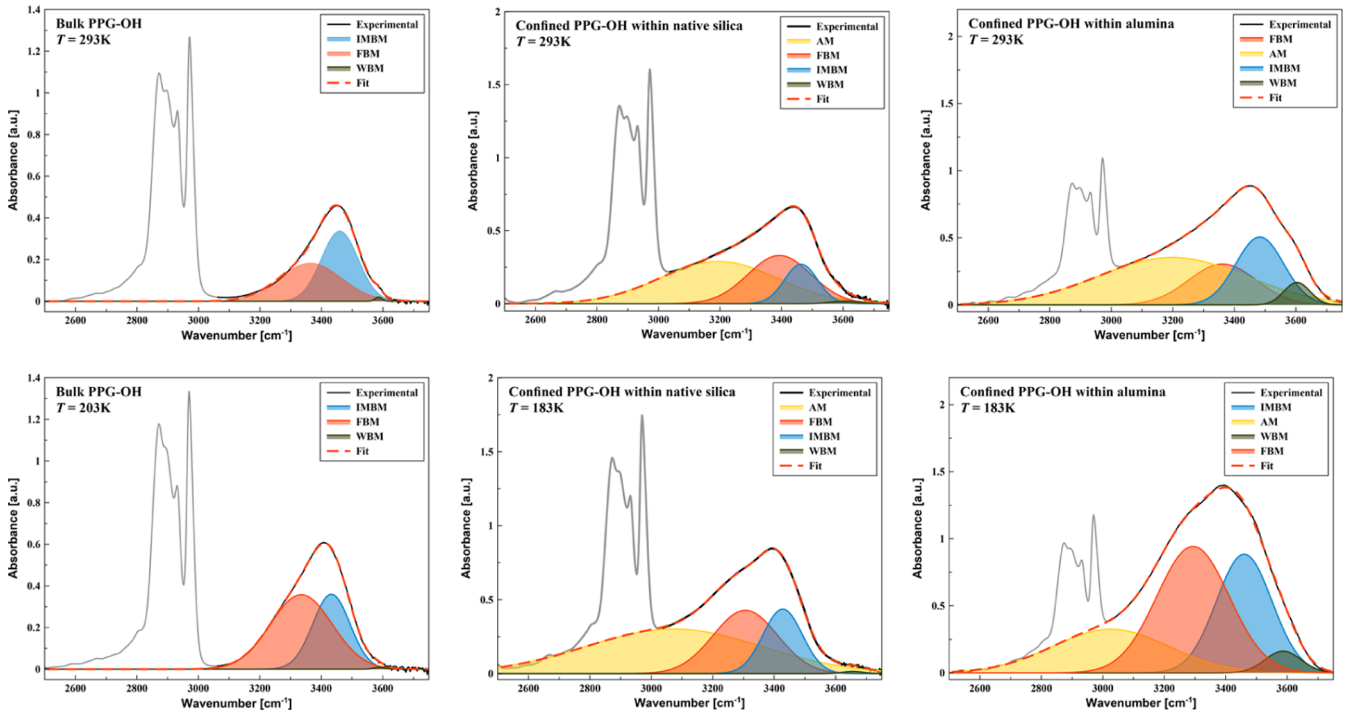

Figure 8. Decomposition of the ν_{OH} band of bulk and confined PPG-OH in the frequency range of 2500 and 3750 cm^{-1} in the temperatures of 293 K and T_g.

and T_g, in the spectral region corresponding to the stretching vibration of the X−H and C−H moieties (3800−2600 cm^{-1}). It should be noted that the FTIR spectral data, especially obtained for alumina pores, were difficult to interpret because of additional strong contribution of the stretching vibrations of the −OH groups of the pore surface to the measured spectra.

An informative band for the analysis of hydrogen bond interactions is that connected to the X−H stretching vibrations of the proton donor groups (the ν_{X-H}). This spectral feature occurs in the range of 3700−3000 cm^{-1} in the FTIR spectra of the studied systems. The band observed between 3000 and 2800 cm^{-1} is responsible for the stretching vibrations of the C−H groups of the carbon skeleton. The position and frequency of the ν_{X-H} bands for the bulk samples differ between PPG-OH and PPG-NH_2 (see Figure 7). At 293 K (room temperature, RT) ν_{O-H} band of bulk PPG-OH occurs as a single broad peak located at 3453 cm^{-1}, whereas the ν_{N-H} band of PPG-NH_2 consists of three peaks at 3369, 3298, and 3201 cm^{-1}. Thus, the H-bonds in both PPG derivatives are of medium strength. The different profiles of the ν_{X-H} band of PPG-OH and PPG-NH_2 correspond to the various types of H-bonded aggregates. Note that it seems that the H-bonded oligomeric structures dominate in PPG-OH, while probably a more complex H-bonding network (the ring- or chain-like structures) can be formed in PPG-NH_2. The spectral modifications of the X−H stretching bands of PPG-OH and PPG-NH_2 accompanying the temperature drop are consistent with the trend reported in the literature and discussed in the Supporting Information file.

In the next step, the FTIR approach was applied to investigate the effects of the nanoconfinement of PPG samples after their incorporation into different nanopore templates (silica and alumina). Representative spectra measured at different temperatures for the sample infiltrated in porous matrices are presented in Figures S4 and S5 in the Supporting Information file. The interaction of PPGs molecules within silica or alumina membranes causes noticeable changes in their IR spectra that represent the change in the hydrogen-bonded pattern in the investigated systems. At RT, the IR spectra of the confined liquids exhibit a significant redshift of the ν_{X-H} peak frequency values, relative to the bulk samples (Figure 7). This spectral effect is associated with the existence of stronger H-bonds in PPGs under nanoconfinement. Similar results are observed in IR spectra measured after the temperature drop. In detail, the larger redshift of the O−H stretching vibrations for PPG-OH molecules is observed for the native pores (14 cm^{-1}) compared to the silanized pores (11 cm^{-1}) or the alumina ones(12 cm^{-1}) at T_g. In the case of PPG-NH_2, the most intense peak of the ν_{N-H} band at 3359 cm^{-1} is shifted by 4 cm^{-1} in native pores and 3 cm^{-1} in silanized pores relative to the bulk at T_g. On the other hand, the ν_{N-H} peak in alumina membranes shows the same position as that in the bulk. Thus, the PPG molecules within silanized silica pores exhibit the smallest spectral changes (*i.e.,* the redshift of the ν_{X-H} peak frequency value) relative to other systems. This is because of the weaker interactions between the host and guest material. It is also observed that the ν_{X-H} bands measured for the confined samples are much broader than those measured for the bulk materials. This indicates that PPG molecules also exhibit greater variability in the size of the H-bonded aggregates in a confined environment. In order to address this issue more carefully, we performed additional analysis relying on the deconvolution of the spectra measured in the 3000−3800 cm^{-1} region for PPG-OH; please see Figures 8 and S6. This oligomer was selected and described in detail because it interacts the most with the native pores. To evaluate the contribution of specific components in this complex spectral regime, data collected for bulk and confined PPG-OH were fitted to the combination of several Gauss functions. The procedure of the fitting of the −OH stretching bands was

https://dx.doi.org/10.1021/acs.jpcc.0c04062
J. Phys. Chem. C 2020, 124, 17607−17621

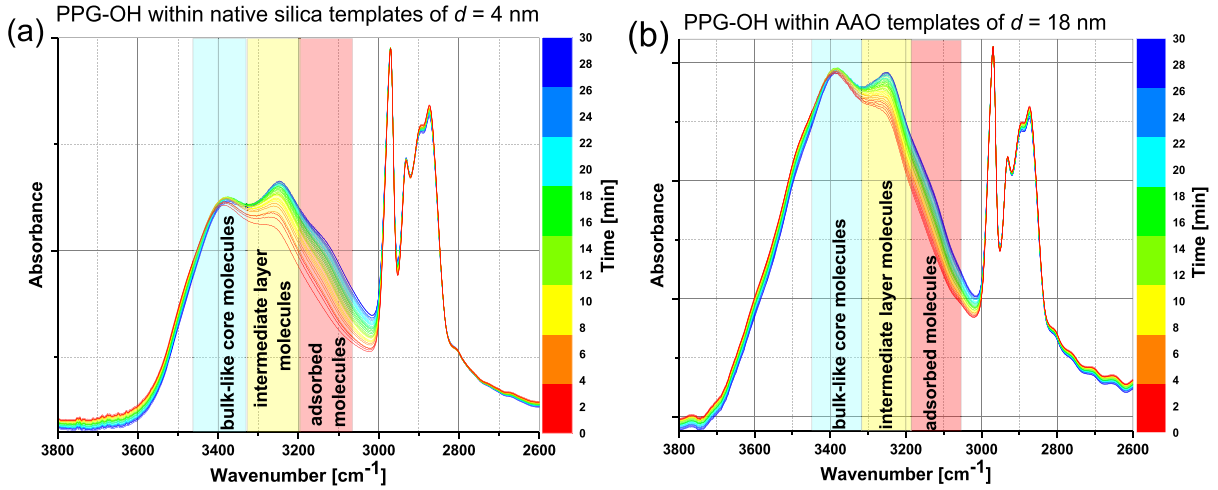

Figure 9. Time-dependent FTIR spectra of confined PPG-OH within the native silica (a) and alumina membranes (b) in the O−H and C−H stretching regions, recorded at 183 K over 30 min. The spectra were normalized to the C−H peak at around 2970 cm^{-1}.

performed following the scheme reported for liquid water in refs.[63,66] This approach allows studying the hydrogen bonding interactions between surface silanol and PPG-OH at the interface. It is worthwhile to point out that H-bonds can be formed between PPG-OH molecules, silanol groups, and the host and guest material *via* the siloxane bridging oxygen group.

The bulk spectrum of PPG-OH in Figure 8 consists of the three Gaussian components assigned to vibration of the OH moiety in the (i) fully H-bonded bulk-like molecules (FBM, 3393−3259 cm^{-1}), (ii) intermediate (partially) H-bonded molecules (IMBM, 3482−3417 cm^{-1}), and (iii) weakly H-bonded molecules (WBM, 3619−3587 cm^{-1}). For the sample confined in pores, an additional Gaussian component is required to describe the FTIR spectra in the 3198−3026 cm^{-1} region. This additional band is assigned to the ν_{OH} in the molecules adsorbed (AM) at the interface. The comparison of the deconvoluted IR spectra in the −OH stretching vibration region for bulk and confined PPG-OH at RT and at T_g is shown in Figures 8 and S6 in the Supporting Information file. Figure S7 illustrates the temperature variations of the spectral parameters such as peak position and integrated areas obtained for each component (fraction of molecule) from the fitting IR spectra of bulk and confined PPG-OH to the superposition of several Gauss functions. All these parameters are also listed in Table S1. On the other hand in Table S2, the percentage areas of the deconvoluted profiles are shown, which give information on the different populations of H-bonded structural arrangements in PPG-OH. From the analysis of the results obtained at T_g (Table S1), one finds a redshift of the maximum of the all fractions of H-bonded oligomers in confined sample with respect to the bulk material. This indicates the enhancement of the H-bonding interactions under confinement. As shown in Figure 8, the largest peak area in bulk sample corresponds to the fully H-bonded PPG-OH molecules. On the other hand, quite a large variety of adsorption behavior of PPG-OH on the different pore walls is observed (Figures 8 and S6). In the native pores, the adsorption process is the most dominant because the AM component has the largest percentage in the OH band profile in selected temperatures. The silanized membranes exhibit similar behavior at higher temperatures; however, below 263 K, partially H-bonded PPG-OH structures predominate. In the case of alumina templates, the AM component also dominates at 293K−233 K, whereas at low temperatures, the interactions between FBM are the strongest.

Next, the change in contribution of various Gaussian components to the overall spectrum upon temperature drops was monitored. As shown in Table S1, the positions of FBM and IMBM substructures are shifted to lower wavenumbers with decreasing temperature, indicating the strengthening of the interactions between "fully" and "partially" H-bonded PPG-OH molecules. On the contrary, the blueshift of the WBM components is observed because of the growth of the degree of association of PPG-OH at T_g. Simultaneously, the integrated area of the FBM and IMBM components increases and the WBM area decreases as the temperature is lowered indicating the growing organization of PPG-OH toward a fully H-bonded network. However, it should be pointed out that the FBM contribution in confined PPG-OH within the silanized silica templates exhibits opposite temperature effect, that is, it decreases with the lowering temperature. More detailed analysis based on the percentage contribution of the Gaussian component areas shows that in bulk PPG-OH, the FBM-type molecules are the dominating population, their proportion steadily increases from 48 to 62% as the temperature decreases from RT to T_g. Interestingly, in all-confined PPG-OH, the AM sub-band has the largest percentage at RT. As the temperature is lowered, the adsorption process is rather reduced in favor of the fully (alumina templates) and partially (silica and alumina templates) H-bonded interactions. The greatest effect of temperature on the adsorption process is observed for the alumina membrane in which the AM contribution decreases from 51 to 23%, while the FBM and IMBM populations increases 20−42 and 24−30%, respectively. Thus, the variations of the respective populations illustrate that for confined materials, the adsorbed PPG-OH molecules are always the dominating population at RT. At T_g, the interfacial H-bonded species are prevailing only in the native silica pores.

As a final point of our investigations, we have performed the time-dependent FTIR measurements on the PPG-OH confined into silica and alumina membranes to verify whether the annealing at $T_{g,core}$ will influence on the H-bonding network. The analysis of these spectra in the ν_{O-H} band region shows both changes in the shape of the band profile and its broadening as a function of time (Figure 9). The peak located around 3400 cm^{-1}, originating from the bulk-like core

https://dx.doi.org/10.1021/acs.jpcc.0c04062
J. Phys. Chem. C 2020, 124, 17607−17621

molecules, essentially shows no variation over time (the light blue area in Figure 9). Simultaneously the strong intensity growth of the sub-band at the lower wavenumber (approximately 3250 cm^{-1}) in both kind of pores (indicated as a light yellow area in Figure 9) was clearly detected. Interestingly, this band has been assigned herein to the vibration of the hydroxyl moiety in FBM. Moreover, IR spectra recorded during annealing also revealed appearance of the sub peak at $\nu_{OH} \sim$ 3120 cm^{-1}connected to the adsorbed molecules. This band is probably because of the formation of the strongest H-bonds between PPG molecules and hydroxyl units attached to the silica and alumina templates (highlighted as light pink area in Figure 9). Growing intensity of the band observed at 3250 cm^{-1} during annealing can be assigned to the formation of an intermediate layer of the molecules located between core and interfacial ones. However, because of overlapping of this band with that originating from the fraction of FBM of the bulk material, it was not possible to detect it in the FTIR spectra measured at different temperatures. Moreover, analysis of the position of the new band at 3120 cm^{-1} indicated stronger interactions between the PPG-OH molecules and the silica surface with respect to the alumina. It is worthy to mention that this oligomer wets the alumina surface much better with respect to the silica one. Hence, it is a clear indication that enhanced wettability does not have to necessarily mean stronger interactions between host and guest material at least in the case of associating H-bonded liquids. Moreover, various strengths of the H-bonds between PPG and hydroxyl moieties attached to the silica and alumina pores suggest different chemical characters of this functional group that affects their different tendencies in formation of these specific interactions in both kinds of materials.

It must be also stressed that above discussed results obtained for confined PPGs differ from those obtained for water or alcohols infiltrated in nanoporous templates. For primary alcohols incorporated to the native and silanized silica pores, we have found that the strength of H-bonds in confined samples was weaker compared to those in bulk systems which was manifested in the IR spectra as the blueshift of the ν_{O-H} peak frequency.[49] In the case of water confined in zeolites, the O−H bands were slightly redshifted with respect to bulk water, indicating, that under confinement, molecules are relatively strongly hydrogen-bonded.[64] Moreover, the IR spectra of water confined in controlled pore glasses proved that this fluid is perturbed on very large scales (more than 10 nm), even in pores of greater diameter (d = 55 nm). The position of the connectivity band (∼150 cm^{-1}) increased when the pore size decreased, suggesting stronger H-bonding interactions between neighboring water molecules. Additionally, an important decrease of the FWHM of the connectivity band was found for the spatially restricted sample (70%) which was related to a different orientation dynamics of water (up to 55 nm) as compared to bulk liquid.[65] Besides, Baum *et al.*[66] highlighted the predominant effect of the pore size, the kosmotropic properties and the surface ions excess on the dynamics, and the structure of water molecules in the pore and within the interfacial layer. The molecular dynamics simulations of the IR spectrum of isotopically dilute HOD in D_2O in 2.4 nm hydrophilic, amorphous silica pores[67] showed that −OH groups are involved in weaker H-bonds to the silica oxygen acceptors than to water, leading to blueshifts in their frequencies, although this spectral effect was not observed in the measured IR spectra. This fact was explained by the smaller transition dipole moments of these −OH groups. Similar results were reported for HDO in H_2O in Aerosol-OT reverse micelles of varying sizes.[68] Although, in this case, the ν_{O-D} bands exhibited a significant blueshift relative to the bulk liquid, indicating a weakening of hydrogen bonds between the OD groups because of the presence of the interface between the water pool and the surfactant headgroups.[67,69] Herein, it is also worth to mention about work by Zanotti *et al.* for water molecules in Vycor (a hydrophilic porous silica glass).[70] They have found the O−H stretching sub-band at 3230 cm^{-1} that was interpreted as a result of the existence of a monolayer of water molecules H-bonded to the silanol (Si−OH) groups of the Vycor surface. The position of this peak revealed that the H-bonds in this system are significantly stronger than in bulk liquid water (around 3400 cm^{-1}). A further more detailed understanding of the molecular interactions of water confined in mesoporous silica was presented by Knight *et al.*[71] The authors fit the O−H stretch region using three Gaussian curves, representing unique water populations, described as network water (NW), intermediate water (IW), and multimer water (MW). However, these studies also showed a systematic blueshift in the IR peak locations of NW, IW, and MW in confined water. The authors suspected that water in pores is congregating around surface hydroxyl groups to form islands of highly coordinated localized regions. Hence, results of Knight *et al.* are similar to those reported herein.[71] However, it is worthwhile to point out that FTIR measurements on PPG confined in either silica or alumina membranes clearly revealed that although there are at least three fractions of molecules differing in the H-bond pattern in these conditions, the strength of these specific interactions is much stronger with respect to the bulk materials.

At the first sight, this experimental finding questions interpretation of the calorimetric data suggesting that there are two fractions of molecules differing in mobility and glass transition temperature discussed in terms of the "two-layer" (or "core−shell") model. However, it must be stressed that a change in the H-bonded pattern does not have to influence dynamics of confined systems to the extent allowing registration of the third glass transition temperature related to the vitrification of the intermediate layer. In this context, one can recall papers devoted to polymer thin films discussing the occurrence of the third (intermediate) layer.[23] As reported, T_g of ultrathin poly(methyl methacrylate) (PMMA) films depends on the type of applied substrates, that is, increasing for silicon oxide (polar surface) because of the hydrogen bonding and decreasing for the nonpolar surface, together with thickness reduction. It was observed that the dynamics and T_g of each layer differ from the corresponding bulk substances. This indicates that the nature of the interaction between materials and interface is one of the dominant factors in determining the glass-transition temperatures that strongly depends on the thickness of the film and the interfacial energy between the polymer and the substrate. Additionally, the formation of the third layer between the adsorbed layer and core volume was investigated for nanopores.[72] Using calorimetric measurements, it was revealed the existence of three T_gs for PMMA confined into AAO nanopores of d = 300 nm, where (i) molecules near interfaces (of T_g higher than for the bulk), (ii) molecules interacting at the center of nanopores (T_g lower than for the bulk), and (iii) fraction located between abovementioned (characterized by intermediate T_g in a nonequilibrium state). Interestingly for PMMA restricted

https://dx.doi.org/10.1021/acs.jpcc.0c04062
J. Phys. Chem. C 2020, 124, 17607−17621

into d = 80 nm of AAO, only double T_gs was noted.[61] Generally, the formation of the third layer was considered as being strictly connected with the weakening of the interfacial effect between polymer matrices together with increasing pore diameter.[23,72] Besides, it was indicated that the existence of the third layer and also the shift of T_g strictly depends on the thermal history (heating/cooling rate, aging/annealing procedure) of the samples and might be strictly correlated with the exchange effects between the adsorbed layer, interlayer (two layers are trapped in a non-equilibrium state), and the core volume.[23,72] Note that recently, the presence of the additional interlayer under confinement was also reported for poly(methylphenylsiloxane) infiltrated into AAO templates, where interestingly, the third T_g was also detected for small pore size, d = 18 nm.[73]

One can also add that the resolving of the intermediate layer within the confined PPGs with time might, in fact, help us to understand better the reported recent shift of the segmental/structural relaxation process of various incorporated materials upon the annealing experiments performed at following temperature conditions, $T_{g,interfacial} > T_{anneal} > T_{g,core}$.[62,74,75] Note that at the studied range of temperatures, the examined systems are highly heterogeneous (the interfacial fraction of molecules is vitrified and the core ones are not). Briefly, as the annealing experiment proceeds, the shift of the α-relaxation peak toward lower frequencies was observed[74,75] resulting in completely different $\tau_\alpha(T)$-dependences of confined materials with respect to the measurements performed prior to annealing (see Figure S8 in the Supporting Information file). As assumed, the density packing of core and interfacial molecules was out of equilibrium, which was recovered upon sample annealing. Consequently, the confined system moves from the one isochoric condition to the other, characterized by different densities and dynamics.[15,41,76] Nevertheless, as indicated by complementary FTIR measurements, the observed variation of structural/segmental dynamics might be also related to the variation of the H-bonding pattern or processes ongoing at the interface. It looks that during the annealing, there is a strong rearrangement of the interfacial layer leading to the formation of strong H-bonds between PPG and either silica or alumina pore walls. Moreover, the enhancement of these specific interactions is accompanied by the formation of the intermediate layer being in some distance from the pore walls.[23,41,72] Thus, in the annealed samples, we can clearly distinguish into three fractions, namely, interfacial, intermediate, and bulk-like fractions of molecules in the liquids infiltrated into pores.

4. CONCLUSIONS

In this work, we investigated the behavior of three various poly(propylene glycol) derivatives of M_n = 400 g/mol characterized by different abilities to form H-bonds and incorporated into alumina (d = 18 nm) and silica (native and silanized of d = 4 nm) templates. These studies enabled us to explore the impact of finite size and surface interactions on the overall behavior of substances in spatially restricted systems. The observed deviation of segmental relaxation times from the bulk-like behavior indicates that independently on the pore diameter and applied templates, they deviate at similar τ_α. Interestingly, we observed that although previous reports suggested that the shift in glass transition temperatures correlates with the interfacial energy and wettability, such relationship does not hold for PPGs infiltrated within alumina (d = 18 nm) and native and functionalized silica (d = 4 nm) templates. It indicates that besides the surface interactions and finite size (curvature), also other factors, that is, specific interactions, and density packing, possibly surface roughness, should also be taken into account when discussing the behavior of the confined liquid. Additionally, for the investigated PPGs, we observed that $T_{g,int}$ occurs even if $T_{g,core}$ has not been reached before, which indicates that $T_{g,core}$ is not a spinodal temperature. Finally, using FTIR spectroscopy, it was also revealed that the strength of hydrogen bond interactions between the incorporated material and interface differs dependently to the applied templates. Moreover, the time-dependent IR spectra recorded during annealing around the $T_{g,core}$ revealed rearrangement in the interfacial layer leading to the formation of very strong H-bonds between PPG and alumina or silica pore walls. Consequently, this simple experiment allowed us to visualize and distinguish an intermediate layer (rarely reported in literature) between interfacial and bulk-like fraction of molecules. This completely new finding might shed new light and allow us to better understand the shift of the structural/segmental relaxation upon annealing below $T_{g,interfacial}$. It seems that variation in the H-bonds and density packing between molecules attached to the interface and the intermediate ones is responsible for this phenomenon.

■ ASSOCIATED CONTENT

Supporting Information

The Supporting Information is available free of charge at https://pubs.acs.org/doi/10.1021/acs.jpcc.0c04062.

Preparation of porous silica templates, DSC thermograms, dielectric loss, and FTIR spectra of empty silica templates, nitrogen adsorption/desorption isotherms measured for native silica templates, dielectric loss spectra of bulk PPGs, dielectric loss spectra collected upon annealing of confined samples, FTIR spectra measured for bulk and confined PPGs, and their decomposition as well as temperature evolution (PDF)

■ AUTHOR INFORMATION

Corresponding Authors

Agnieszka Talik − *Institute of Physics and Silesian Center of Education and Interdisciplinary Research, University of Silesia in Katowice, 41-500 Chorzow, Poland;* orcid.org/0000-0001-7940-6967; Email: agnieszka.talik@smcebi.edu.pl

Magdalena Tarnacka − *Institute of Physics and Silesian Center of Education and Interdisciplinary Research, University of Silesia in Katowice, 41-500 Chorzow, Poland;* orcid.org/0000-0002-9444-3114; Email: magdalena.tarnacka@smcebi.edu.pl

Barbara Hachuła − *Institute of Chemistry, University of Silesia in Katowice, 40-006 Katowice, Poland;* Email: barbara.hachula@us.edu.pl

Authors

Monika Geppert-Rybczyńska − *Institute of Chemistry, University of Silesia in Katowice, 40-006 Katowice, Poland;* orcid.org/0000-0002-7112-9624

Kamil Kaminski − *Institute of Physics and Silesian Center of Education and Interdisciplinary Research, University of Silesia in Katowice, 41-500 Chorzow, Poland;* orcid.org/0000-0002-5871-0203

https://dx.doi.org/10.1021/acs.jpcc.0c04062
J. Phys. Chem. C 2020, 124, 17607−17621

Marian Paluch − *Institute of Physics and Silesian Center of Education and Interdisciplinary Research, University of Silesia in Katowice, 41-500 Chorzow, Poland*

Complete contact information is available at: https://pubs.acs.org/10.1021/acs.jpcc.0c04062

Notes

The authors declare no competing financial interest.

■ ACKNOWLEDGMENTS

M.T., M.P., and K.K. is thankful for financial support from the Polish National Science Centre within the OPUS project (Dec. no. 2019/33/B/ST3/00500).

■ REFERENCES

(1) Arndt, M.; Stannarius, R.; Gorbatschow, W.; Kremer, F. Dielectric investigations of the dynamic glass transition in nanopores. *Phys. Rev. E: Stat. Phys., Plasmas, Fluids, Relat. Interdiscip. Top.* **1996**, *54*, 5377−5390.

(2) Suzuki, Y.; Duran, H.; Steinhart, M.; Butt, H.-J.; Floudas, G. Suppression of Poly(ethylene oxide) Crystallization in Diblock Copolymers of Poly(ethylene oxide)-b-poly(ε-caprolactone) Confined to Nanoporous Alumina. *Macromolecules* **2014**, *47*, 1793−1800.

(3) Jasiurkowska-Delaporte, M.; Kossack, W.; Kipnusu, W. K.; Sangoro, J. R.; Iacob, C.; Kremer, F. Glassy dynamics of two poly(ethylene glycol) derivatives in the bulk and in nanometric confinement as reflected in its inter- and intra-molecular interactions. *J. Chem. Phys.* **2018**, *149*, 064501.

(4) Iacob, C.; Sangoro, J. R.; Papadopoulos, P.; Schubert, T.; Naumov, S.; Valiullin, R.; Kärger, J.; Kremer, F. Charge transport and diffusion of ionic liquids in nanoporous silica membranes. *Phys. Chem. Chem. Phys.* **2010**, *12*, 13798−13803.

(5) Kipnusu, W. K.; Elsayed, M.; Krause−Rehberg, R.; Kremer, F. Glassy dynamics of polymethylphenylsiloxane in one- and two-dimensional nanometric confinement—A comparison. *J. Chem. Phys.* **2017**, *146*, 203302.

(6) Kipnusu, W. K.; Elmahdy, M. M.; Elsayed, M.; Krause-Rehberg, R.; Kremer, F. Counterbalance between Surface and Confinement Effects As Studied for Amino-Terminated Poly(propylene glycol) Constraint in Silica Nanopores. *Macromolecules* **2019**, *52*, 1864−1873.

(7) Huwe, A.; Arndt, M.; Kremer, F.; Haggenmüller, C.; Behrens, P. Dielectric Investigations of the Molecular Dynamics of Propanediol in Mesoporous Silica Materials. *J. Chem. Phys.* **1997**, *107*, 9699.

(8) Kipnusu, W. K.; Elsayed, M.; Kossack, W.; Pawlus, S.; Adrjanowicz, K.; Tress, M.; Mapesa, E. U.; Krause-Rehberg, R.; Kaminski, K.; Kremer, F. Confinement for More Space: A Larger Free Volume and Enhanced Glassy Dynamics of 2-ethyl-1-hexanol in Nanopores. *J. Phys. Chem. Lett.* **2015**, *6*, 3708−3712.

(9) Wubbenhorst, M.; Lupascu, V. Glass Transition Effects in Ultra-Thin Polymer Films Studied by Dielectric Spectroscopy - Chain Confinement vs. Finite Size Effects. *2005, 12th International Symposium on Electrets*, 2005.

(10) White, R. P.; Lipson, J. E. G. Polymer Free Volume and Its Connection to the Glass Transition. *Macromolecules* **2016**, *49*, 3987−4007.

(11) White, R. P.; Lipson, J. E. G. How Free Volume Does Influence the Dynamics of Glass Forming Liquids. *ACS Macro Lett.* **2017**, *6*, 529−534.

(12) White, R. P.; Lipson, J. E. G. Connecting Pressure-Dependent Dynamics to Dynamics under Confinement: The Cooperative Free Volume Model Applied to Poly(4-chlorostyrene) Bulk and Thin Films. *Macromolecules* **2018**, *51*, 7924−7941.

(13) Panagopoulou, A.; Rodríguez-Tinoco, C.; White, R. P.; Lipson, J. E. G.; Napolitano, S. Substrate Roughness Speeds Up Segmental Dynamics of Thin Polymer Films. *Phys. Rev. Lett.* **2020**, *124*, 027802.

(14) Adrjanowicz, K.; Kaminski, K.; Koperwas, K.; Paluch, M. Negative Pressure Vitrification of the Isochorically Confined Liquid in Nanopores. *Phys. Rev. Lett.* **2015**, *115*, 265702.

(15) Tarnacka, M.; Kipnusu, W. K.; Kaminska, E.; Pawlus, S.; Kaminski, K.; Paluch, M. The peculiar Behavior of Molecular Dynamics of Glass-forming Liquid Confined in the Native Porous Materials - The Role of Negative Pressure. *Phys. Chem. Chem. Phys.* **2016**, *18*, 23709−23714.

(16) Szklarz, G.; Adrjanowicz, K.; Tarnacka, M.; Pionteck, J.; Paluch, M. Confinement-Induced Changes in the Glassy Dynamics and Crystallization Behavior of Supercooled Fenofibrate. *J. Phys. Chem. C* **2018**, *122*, 1384−1395.

(17) Napolitano, S.; Rotella, C.; Wübbenhorst, M. Can Thickness and Interfacial Interactions Univocally Determine the Behavior of Polymers Confined at the Nanoscale? *ACS Macro Lett.* **2012**, *1*, 1189−1193.

(18) Napolitano, S.; Lupaşcu, V.; Wübbenhorst, M. Temperature dependence of the deviation from bulk behaviour in ultrathin polymer films. *Macromolecules* **2008**, *41*, 1061−1063.

(19) Rotella, C.; Napolitano, S.; Vandendriessche, S.; Valev, V. K.; Verbiest, T.; Larkowska, M.; Kucharski, S.; Wübbenhorst, M. Adsorption Kinetics Of Ultrathin Polymer Films In The Melt Probed By Dielectric Spectroscopy And Second-Harmonic Generation. *Langmuir* **2011**, *27*, 13533.

(20) Torres, J. A.; Nealey, P. F.; de Pablo, J. J. Molecular Simulation of Ultrathin Polymeric Films near the Glass Transition. *Phys. Rev. Lett.* **2000**, *85*, 3221−3224.

(21) Alexandris, S.; Papadopoulos, P.; Sakellariou, G.; Steinhart, M.; Butt, H.-J.; Floudas, G. Interfacial Energy and Glass Temperature of Polymers Confined to Nanoporous Alumina. *Macromolecules* **2016**, *49*, 7400−7414.

(22) Tarnacka, M.; Wojtyniak, M.; Brzózka, A.; Talik, A.; Hachuła, B.; Kaminska, E.; Sulka, G.; Kaminski, K.; Paluch, M. The Unique Behavior of Poly(propylene glycols) Confined within Alumina Templates Having Nanostructured Interface. *Nano Lett.*, Publication Date: June 19, **2020**.

(23) Fryer, D. S.; Peters, R. D.; Kim, E. J.; Tomaszewski, J. E.; de Pablo, J. J.; Nealey, P. F.; White, C. C.; Wu, W.-L. Dependence of the Glass Transition Temperature of Polymer Films on Interfacial Energy and Thickness. *Macromolecules* **2001**, *34*, 5627−5634.

(24) Lang, R. J.; Merling, W. L.; Simmons, D. S. Combined Dependence of Nanoconfined Tg on Interfacial Energy and Softness of Confinement. *ACS Macro Lett.* **2014**, *3*, 758−762.

(25) Talik, A.; Tarnacka, M.; Geppert-Rybczynska, M.; Minecka, A.; Kaminska, E.; Kaminski, K.; Paluch, M. Impact of the Interfacial Energy and Density Fluctuations on the Shift of the Glass-Transition Temperature of Liquids Confined in Pores. *J. Phys. Chem. C* **2019**, *123*, 5549−5556.

(26) Talik, A.; Tarnacka, M.; Wojtyniak, M.; Kaminska, E.; Kaminski, K.; Paluch, M. The influence of the nanocurvature on the surface interactions and molecular dynamics of model liquid confined in cylindrical pores. *J. Mol. Liq.* **2020**, *298*, 111973.

(27) Tolman, R. C. The Effect of Droplet Size on Surface Tension. *J. Chem. Phys.* **1949**, *17*, 333.

(28) Tolman, R. C. The Superficial Density of Matter at a Liquid-Vapor Boundary. *J. Chem. Phys.* **1949**, *17*, 118.

(29) Simavilla, D. N.; Huang, W.; Housmans, C.; Sferrazza, M.; Napolitano, S. Taming the Strength of Interfacial Interactions via Nanoconfinement. *ACS Cent. Sci.* **2018**, *4*, 755−759.

(30) Schönhals, A.; Goering, H.; Schick, Ch. Segmental and chain dynamics of polymers: from the bulk to the confined state. *J. Non-Cryst. Solids* **2002**, *305*, 140−149.

(31) Schönhals, A.; Stauga, R. Dielectric Normal Mode Relaxation of Poly(propylene glycol) Melts in Confining Geometries. *J. Non-Cryst. Solids* **1998**, *235−237*, 450−456.

(32) Schönhals, A.; Stauga, R. Broadband Dielectric Study of Anomalous Diffusion in a Poly(propylene glycol) Melt Confined to Nanopores. *J. Chem. Phys.* **1998**, *108*, 5130−5136.

(33) Aasen, A.; Blokhuis, E. M.; Wilhelmsen, Ø. Tolman lengths and rigidity constants of multicomponent fluids: Fundamental theory and numerical examples. *J. Chem. Phys.* **2018**, *148*, 204702.
(34) Gibbs, J. W. *The Collected Works*; Longmans Green and Company: New York, 1928; Vol. *I*, p 219.
(35) Blokhuis, E. M.; Kuipers, J. Thermodynamic expressions for the Tolman length. *J. Chem. Phys.* **2006**, *124*, 074701.
(36) Stepanov, S. V.; Byakov, V. M.; Stepanova, O. P. The Determination of Microscopic Surface Tension of Liquids with a Curved Interphase Boundary by Means of Positron Spectroscopy. *Russ. J. Phys. Chem.* **2000**, *74*, S65−S77.
(37) https://www.inredox.com, accessed: 10.02.2020.
(38) Ngo, D.; Liu, H.; Chen, Z.; Kaya, H.; Zimudzi, T. J.; Gin, S.; Mahadevan, T.; Du, J.; Kim, S. H. Hydrogen bonding interactions of H2O and SiOH on a boroaluminosilicate glass corroded in aqueous solution. *npj Mater. Degrad.* **2020**, *4*, 1−14.
(39) Wandschneider, A.; Lehmann, J. K.; Heintz, A. Surface Tension and Density of Pure Ionic Liquids and Some Binary Mixtures with 1-propanol and 1-butanol. *J. Chem. Eng. Data* **2008**, *53*, 596−599.
(40) Feder-Kubis, J.; Geppert-Rybczyńska, M.; Musiał, M.; Talik, E.; Guzik, A. Exploring the Surface Activity of a Homologues Series of Functionalized Ionic Liquids with a Natural Chiral Substituent: (−)-Menthol in a Cation. *Colloids Surf., A* **2017**, *529*, 725−732.
(41) Tarnacka, M.; Talik, A.; Kamińska, E.; Geppert-Rybczyńska, M.; Kaminski, K.; Paluch, M. The Impact of Molecular Weight on the Behavior of Poly(propylene glycols) Derivatives Confined within Alumina Templates. *Macromolecules* **2019**, *52*, 3516−3529.
(42) Alexandris, S.; Sakellariou, G.; Steinhart, M.; Floudas, G. Dynamics of Unentangled cis-1,4-Polyisoprene Confined to Nanoporous Alumina. *Macromolecules* **2014**, *47*, 3895−3900.
(43) Havriliak, S.; Negami, S. A. Complex Plane Analysis of α-dispersions in Some Polymer Systems. *J. Polym. Sci., Part C: Polym. Symp.* **1966**, *14*, 99−117.
(44) Kremer, F.; Schonhals, A. *Broadband Dielectric Spectroscopy*; Springer: Berlin, 2003.
(45) Arndt, M.; Stannarius, R.; Groothues, H.; Hempel, E.; Kremer, F. Length Scale of Cooperativity in the Dynamic Glass Transition. *Phys. Rev. Lett.* **1997**, *79*, 2077.
(46) Kuon, N.; Milischuk, A. A.; Ladanyi, B. M.; Flenner, E. Self-intermediate scattering function analysis of supercooled water confined in hydrophilic silica nanopores. *J. Chem. Phys.* **2017**, *146*, 214501.
(47) Hassion, F. X.; Cole, R. H. Dielectric Properties of Liquid Ethanol and 2-Propanol. *J. Chem. Phys.* **1955**, *23*, 1756.
(48) Hansen, C.; Stickel, F.; Berger, T.; Richert, R.; Fischer, E. W. Dynamics of glass-forming liquids. III. Comparing the dielectric α- and β-relaxation of 1-propanol and o-terphenyl. *J. Chem. Phys.* **1997**, *107*, 1086.
(49) Talik, A.; Tarnacka, M.; Geppert-Rybczyńska, M.; Hachuła, B.; Bernat, R.; Chrzanowska, A.; Kaminski, K.; Paluch, M. Are hydrogen supramolecular structures being suppressed upon nanoscale confinement? The case of monohydroxy alcohols. *J. Colloid Interface Sci.* **2020**, *576*, 217−229.
(50) Tu, W.; Chat, K.; Szklarz, G.; Laskowski, L.; Grzybowska, K.; Paluch, M.; Richert, R.; Adrjanowicz, K. Dynamics of Pyrrolidinium-Based Ionic Liquids under Confinement. II. The Effects of Pore Size, Inner Surface, and Cationic Alkyl Chain Length. *J. Phys. Chem. C* **2020**, *124*, 5395−5408.
(51) Kremer, F. *Dynamics in Geometrical Confinement*; Springer: Cham, Switzerland, 2014.
(52) Vogel, H. Temperatura bhangigkeitgesetz der Viskosität von Flüssigkeiten. *Phys. Z.* **1921**, *22*, 645−646.
(53) Fulcher, G. S. Analysis of Recent Measurements of the Viscosity of Glasses. *J. Am. Ceram. Soc.* **1925**, *8*, 339−355.
(54) Tammann, G.; Hesse, W. Die Abhängigkeit der Viscosität von der Temperatur bie unterkühlten Flüssigkeiten. *Z. Anorg. Allg. Chem.* **1926**, *156*, 245−257.
(55) Young, T. III. An essay on the cohesion of fluids. *Philos. Trans. R. Soc. London* **1805**, *95*, 65−87.
(56) Fowkes, F. M. Attractive forces and interfaces. *Ind. Eng. Chem.* **1964**, *56*, 40−52.
(57) Fowkes, F. M. Determination of interfacial tensions, contact angles, and dispersion forces in surfaces by assuming additivity of intermolecular interactions in surfaces. *J. Phys. Chem.* **1962**, *66*, 382.
(58) Politidis, C.; Alexandris, S.; Sakellariou, G.; Steinhart, M.; Floudas, G. Dynamics of Entangled *cis*-1,4-Polyisoprene Confined to Nanoporous Alumina. *Macromolecules* **2019**, *52*, 4185−4195.
(59) Talik, A.; Tarnacka, M.; Grudzka-Flak, I.; Maksym, P.; Geppert-Rybczynska, M.; Wolnica, K.; Kaminska, E.; Kaminski, K.; Paluch, M. The Role of Interfacial Energy and Specific Interactions on the Behavior of Poly(propylene glycol) Derivatives under 2D Confinement. *Macromolecules* **2018**, *51*, 4840−4852.
(60) Park, J.-Y.; McKenna, G. B. Size and Confinement Effects on the Glass Transition Behavior of Polystyrene/o-Terphenyl Polymer Solutions. *Phys. Rev. B: Condens. Matter Mater. Phys.* **2000**, *61*, 6667.
(61) Li, L.; Zhou, D.; Huang, D.; Xue, G. Double Glass Transition Temperatures of Poly(methyl methacrylate) Confined in Alumina Nanotube Templates. *Macromolecules* **2013**, *47*, 297−303.
(62) Tarnacka, M.; Madejczyk, O.; Kaminski, K.; Paluch, M. Time and Temperature as Key Parameters Controlling Dynamics and Properties of Spatially Restricted Polymers. *Macromolecules* **2017**, *50*, 5188−5193.
(63) Brubach, J.-B.; Mermet, A.; Filabozzi, A.; Gerschel, A.; Roy, P. Signatures of the Hydrogen Bonding in the Infrared Bands of Water. *J. Chem. Phys.* **2005**, *122*, 184509.
(64) Crupi, V.; Longo, F.; Majolino, D.; Venuti, V. Dependence of Vibrational Dynamics of Water in Ion-Exchanged Zeolites A: A Detailed Fourier Transform Infrared Attenuated Total Reflection Study. *J. Chem. Phys.* **2005**, *123*, 154702.
(65) Le Caër, S.; Pin, S.; Esnouf, S.; Raffy, Q.; Renault, J. P.; Brubach, J.-B.; Creff, G.; Roy, P. A Trapped Water Network in Nanoporous Material: The Role of Interfaces. *Phys. Chem. Chem. Phys.* **2011**, *13*, 17658.
(66) Baum, M.; Rieutord, F.; Juranyi, F.; Rey, C.; Rébiscoul, D. Dynamical and Structural Properties of Water in Silica Nanoconfinement: Impact of Pore Size, Ion Nature, and Electrolyte Concentration. *Langmuir* **2019**, *35*, 10780.
(67) Burris, P. C.; Laage, D.; Thompson, W. H. Simulations of the infrared, Raman, and 2D-IR photon echo spectra of water in nanoscale silica pores. *J. Chem. Phys.* **2016**, *144*, 194709.
(68) Moilanen, D. E.; Fenn, E. E.; Wong, D.; Fayer, M. D. Water dynamics in large and small reverse micelles: From two ensembles to collective behavior. *J. Chem. Phys.* **2009**, *131*, 014704.
(69) Thompson, W. H. Perspective: Dynamics of confined liquids. *J. Chem. Phys.* **2018**, *149*, 170901.
(70) Zanotti, J.-M.; Judeinstein, P.; Dalla-Bernardina, S.; Creff, G.; Brubach, J.-B.; Roy, P.; Bonetti, M.; Ollivier, J.; Sakellariou, D.; Bellissent-Funel, M.-C. Competing coexisting phases in 2D water. *Sci. Rep.* **2016**, *6*, 25938.
(71) Knight, A. W.; Kalugin, N. G.; Coker, E.; Ilgen, A. G. Water properties under nano-scale confinement. *Sci. Rep.* **2019**, *9*, 8246.
(72) Li, L.; Chen, J.; Deng, W.; Zhang, C.; Sha, Y.; Cheng, Z.; Xue, G.; Zhou, D. Glass Transitions of Poly(methyl methacrylate) Confined in Nanopores: Conversion of Three- and Two-Layer Models. *J. Phys. Chem. B* **2015**, *119*, 5047−5054.
(73) Adrjanowicz, K.; Winkler, R.; Chat, K.; Duarte, D. M.; Tu, W.; Unni, A. B.; Paluch, M.; Ngai, K. L. Study of Increasing Pressure and Nanopore Confinement Effect on the Segmental, Chain, and Secondary Dynamics of Poly(methylphenylsiloxane). *Macromolecules* **2019**, *52*, 3763−3774.
(74) Tarnacka, M.; Kaminski, K.; Mapesa, E. U.; Kaminska, E.; Paluch, M. Studies on the Temperature and Time Induced Variation in the Segmental and Chain Dynamics in Poly(propylene glycol) Confined at the Nanoscale. *Macromolecules* **2016**, *49*, 6678−6686.
(75) Shi, G.; Guan, Y.; Liu, G.; Müller, A. J.; Wang, D. Segmental Dynamics Govern the Cold Crystallization of Poly(lactic acid) in Nanoporous Alumina. *Macromolecules* **2019**, *52*, 6904−6912.

https://dx.doi.org/10.1021/acs.jpcc.0c04062
J. Phys. Chem. C 2020, 124, 17607−17621

(76) Adrjanowicz, K.; Paluch, M. Discharge of the Nanopore Confinement Effect on the Glass Transition Dynamics via Viscous Flow. *Phys. Rev. Lett.* **2019**, *122*, 176101.

https://dx.doi.org/10.1021/acs.jpcc.0c04062
J. Phys. Chem. C 2020, 124, 17607−17621